SPANWISE WALL OSCILLATION APPLIED TO EXACT COHERENT STATES OF PLANE COUETTE FLOW

Yacine Bengana
Department of Aeronautics
Imperial College London
South Kensington, London SW7 2AZ, UK
y.bengana14@imperial.ac.uk

Qiang Yang
State Key Laboratory of Aerodynamics
China Aerodynamics Research and Development Centre
Mianyang 621000, PR China
qiang.yang@skla.cardc.cn

Yongyun Hwang
Department of Aeronautics
Imperial College London
South Kensington, London SW7 2AZ, UK
y.hwang@imperial.ac.uk

ABSTRACT

The effect of spanwise wall oscillation on exact coherent states in plane Couette flow is investigated for a large range of amplitudes (A_w) and periods of oscillations (T). The control forms a time-dependent shear layer, found responsible for a significant drag reduction of the upper branches of equilibrium solutions. On the other hand, it has only a minor effect on the lower branches. Increasing the oscillation amplitude decreases the skin-friction drag gradually and increases the stabilisation effect. The analysis of phase portraits reveals that the wall oscillation reduces the size of the turbulent region in state space and damps the repelling strength of the upper branch solutions. Moreover, this modification of state-space dynamics by spanwise wall oscillation stabilises most of the equilibrium solutions' unstable modes and shortens the turbulence lifetime significantly.

INTRODUCTION

The skin-friction drag reduction in wall-bounded shear flows is one of the main goals for many engineering designs. Most of the skin-friction drag in such flows is related to the turbulence generation mechanism near the wall especially at low Reynolds numbers. This mechanism, known as the self-sustaining process (Hamilton *et al.*, 1995), is a quasi-cyclic process of alternating quasi-streamwise vortices and high/low-speed streaks. The quasi-streamwise vortices give rise to the streaks through the lift-up mechanism (e.g. Butler & Farrell, 1993). The streaks subsequently experience an instability or a transient growth, which causes their breakdown. Finally, after this breakdown, the quasi-streamwise vortices are regenerated. During the formation of the streaks, the lift-up effect brings a high streamwise momentum to the wall, responsible for a large part of skin-friction production (Kravchenko *et al.*, 1993). Therefore, for the purpose of drag reduction at least at low Reynolds numbers, it is relevant to act on the flow structures in the vicinity of the wall.

There are various strategies for turbulent skin-friction drag reduction in near-wall turbulence. In this paper, we will focus on the spanwise wall oscillation, which forms an unsteady shear layer (i.e. Stokes layer) that interacts with the near-wall structures and can significantly reduce turbulent skin-friction (Jung *et al.*, 1992; Ricco *et al.*, 2021). We define skin-friction drag reduction as the relative difference of skin friction coefficient of the controlled and uncontrolled states. At low Reynolds numbers ($Re_\tau \simeq 200$, where Re_τ is the friction Reynolds number), the spanwise wall oscillation can reduce the skin-friction drag up to 40% with the optimal period $T^+ \approx 100$. The skin-friction decreases as the amplitude of oscillation A_w^+ is increased monotonically.

The main goal of this study is to characterize the state-space dynamics of near-wall turbulence under spanwise wall oscillation control. It has been shown that state-space dynamics may be an important concept to understand and optimize the control of turbulent flow (Kawahara, 2005; Ibrahim *et al.*, 2019). The state space is characterised by various invariant solutions (e.g. equilibria, traveling waves, periodic orbits, etc.), which form the skeleton of its dynamics. In particular, the sustaining actuation like spanwise wall oscillation would deform the entire state space. As such, the examination of how the control changes the invariant solutions would provide physical insight into the state-space dynamics to understand and improve the given control strategy in wall-bounded shear flows.

PROBLEM FORMULATION AND METHOD

We consider the canonical plane Couette flow of incompressible viscous fluid confined between two parallel impermeable plates. We denote x, y and z by the streamwise, wall-normal and spanwise directions, respectively. The upper and lower walls are located at $y = \pm h$, and the flow is driven by imposing the following boundary conditions: $u|_{y=\pm h} = \pm U_w$, where u is the streamwise velocity and $\pm U_w$ the moving velocity of the upper and lower walls. We define the Reynolds number as $Re = U_w h / \nu$, where ν is the kinematic viscosity.

The numerical simulations are carried out using the Navier-Stokes solver `Diablo` (Bewley, 2014). In this code, we use a second-order central differences scheme and Fourier series with $2/3$ dealiasing rule to discretize the wall-normal and periodic directions respectively. A combination of the

Crank-Nicolson and third-order Runge-Kutta method serves for time integration. We considered two flow domains $\Omega_N \equiv [L_x/h \; L_y/h \; L_z/h] = [1.75\pi \; 2 \; 1.2\pi]$ and $\Omega_{HKW} = [3.4662\pi \; 2 \; 1.7391\pi]$. The periodic boundary condition is imposed in the wall-parallel directions. The spanwise wall-oscillation control is implemented, so that the two walls oscillate in phase in the spanwise direction according to

$$W_w(t) = A_w \sin(\omega t) = A_w \sin(2\pi t/T), \qquad (1)$$

where W_w is the spanwise velocity at the wall, A_w the amplitude, T the wall oscillation period, and ω the angular frequency. The parameters are scaled with inner viscous units of the uncontrolled turbulent state at $Re = 400$: i.e. $A_w^+ = A_w/u_\tau$ and $T^+ = T u_\tau^2/\nu$, where $u_\tau = \sqrt{\tau_w/\rho}$ is the skin-friction velocity with τ_w being the wall-shear stress of the uncontrolled flow. The skin-friction coefficient is defined as $C_f = 2(Re_\tau/Re)^2$, where $Re_\tau = u_\tau h/\nu$ is the friction Reynolds number.

In the present study, we consider four sets of equilibrium solutions, i.e. EQ0 obtained in Ω_N by Nagata (1990), EQ1, EQ4 and EQ7 obtained in Ω_{HKW} by Gibson $et\ al.$ (2009). The edge state is a periodic orbit (PO) identical to the gentle periodic solution found by Kawahara & Kida (2001). Depending on the skin-friction value, the solutions are classified into lower (low friction) and upper (high friction) branches (see below for further details). The solutions are computed using the Newton-Krylov-Hookstep method, which minimizes the relative error between the initial state and the final state translated in time and streamwise direction at $t = T_0$. When there is no control, the equilibrium states considered are stationary. Therefore, the period T_0 can arbitrarily be fixed, and $T_0 = 8h/U_w$ is used in the present study. However, under spanwise wall oscillation control, the period needs to satisfy $T_0 = nT$, where a positive integer number n is fixed as $n = 1$ to minimize the computational cost. Once an equilibrium solution is obtained, its bifurcation is also studied. To construct the bifurcation diagrams, the continuation with the Reynolds number Re or the control parameters A_w and T of the solutions is carried out using pseudo-arc-length continuation which improves the computation of the equilibrium solutions near turning points. Finally, the stability of each equilibrium solution is examined using the standard Arnoldi iteration.

RESULTS AND DISCUSSION
Bifurcation overview

The bifurcation diagram, represented by $C_f - Re$, of the equilibrium solutions and edge state, is shown in figure 1. Each solution arise from a saddle-node bifurcation. The solution EQ0, discovered by Nagata (1990), appears at the smallest critical Reynolds number $Re_c \approx 127$, then followed by EQ7 at $Re_c \approx 167$ from Gibson $et\ al.$ (2009). The bifurcation curves for EQ1 and EQ4 show several bifurcations. EQ1 exhibits a series of sophisticated saddle-node bifurcations in which the four branches twisted one another. The first saddle-node bifurcation occurs at $Re_c \approx 386$, and the second and third bifurcations occur on the upper branch at $Re_c = 408$ and $Re_c = 435$, respectively. EQ4 arises from a saddle-node bifurcation at $Re_c = 275$, followed by a second from the lower and upper branch at $Re_c = 494$ and $Re_c = 438$, respectively. The bifurcation curve of PO has a critical Reynolds number located at $Re_c = 236$. To analyse the action of control on the bifurcation curves, we focus only on the equilibrium solution EQ0. The other solutions show similar behaviours.
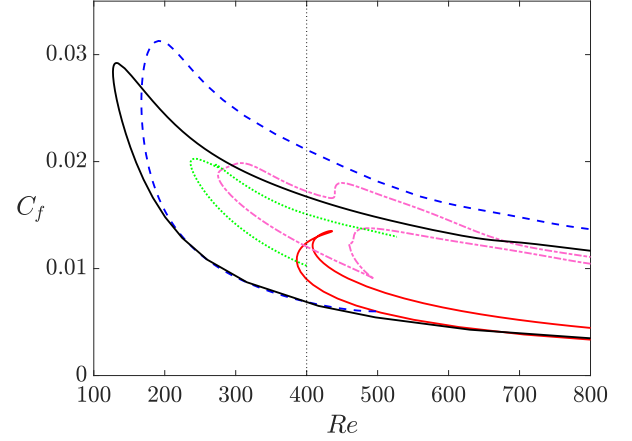

Figure 1. Bifurcation diagram of the equilibrium solutions and periodic orbit: EQ0, black thick solid line; EQ1, red solid line; EQ4, pink dash-dotted line; EQ7, blue dashed line; PO, green dotted line. The vertical dotted line indicates $Re = 400$.

Previous studies have shown that spanwise wall oscillation reaches the optimal of drag reduction at $T^+ \approx 100$. Figure 2(a) shows the bifurcation curves for EQ0 for different oscillation periods $T^+ \in [0, 300]$ at a fixed wall oscillation amplitude $A_w^+ = 0.85$. In this figure, we focus on the identification of the saddle-node point. Therefore, for this figure, we use the viscous inner units of the uncontrolled saddle-node point for the scaling of the oscillation period. The control reduces the skin-friction drag for the upper branch significantly, while it has a minor effect on the lower solution. The saddle-node point is continuously pushed to higher Re as the oscillation period T^+ is increased, from $Re_c = 127.3$ at $T^+ = 0$ to $Re_c = 142.5$ at $T^+ = 211.9$. We note that at $T^+ = 264.9$ the saddle-node point decreases to $Re_c = 142.2$ and increases only slightly for $T^+ > 106$. Those observations indicate an optimal oscillation period around $T^+ = 100$, consistent with the DNS data as well as our previous bifurcation study of the ECS under spanwise wall oscillation in Poiseuille flow (Yang $et\ al.$, 2019). Figure 2(b) shows the bifurcation curves of the equilibrium solution EQ0 for different spanwise wall oscillation amplitudes at fixed wall oscillation period $T^+ = 79.8$. The solid line indicates the uncontrolled reference case. When increasing A_w^+, the upper branch shows a significant drag reduction. The strong control effect on the upper branch involves a substantial change in the bifurcation diagram by introducing new bifurcations along the upper branch. On the contrary, the effect on the lower branch is nearly negligible over almost the entire range of Re. The effect of the control is, however, not monotonic. Indeed, near the bifurcation point, the skin-friction drag of the lower branch is slightly increased. Therefore, the two branches are pushed towards each other until they merge and disappear. The consequence is that the control pushes the threshold of the saddle-node bifurcations to higher Reynolds numbers, which indicates a stabilisation of the equilibrium solutions. Figure 2(c) shows the bifurcation curves of the skin-friction coefficient to the wall oscillation amplitude A_w^+ for various oscillation periods T^+ at a fixed $Re = 400$. The upper branch exhibits a significant reduction of skin friction when increasing A_w^+, which is consistent with figure 2(b). On the other hand, C_f of the lower branch depends on each solution and the period of oscillation considered. Therefore the two branches converge and meet at a given value of A_w^+, forming a saddle-node bifurcation
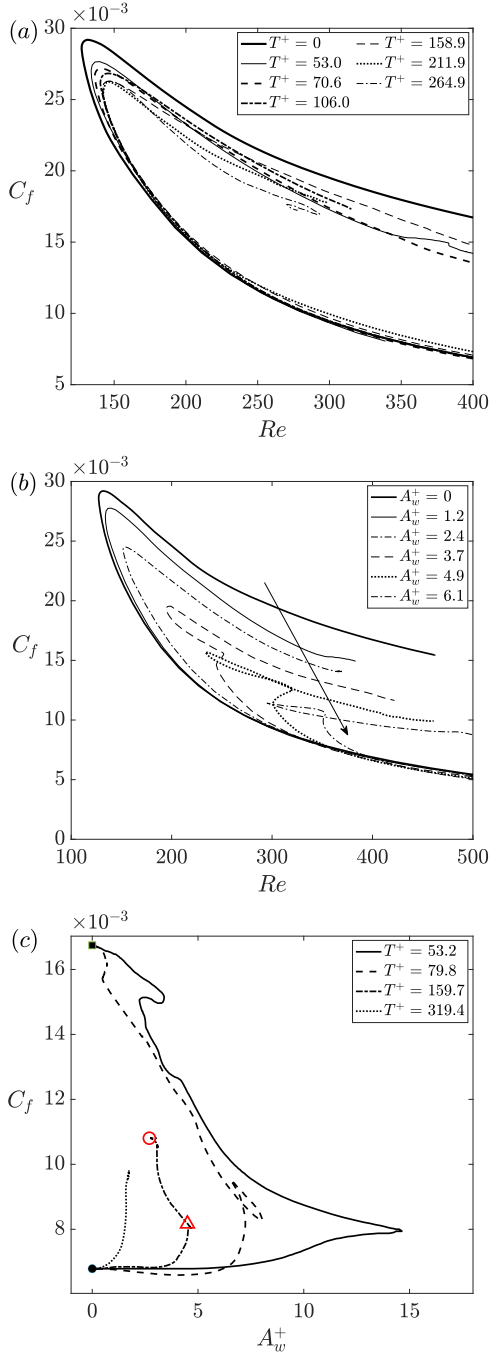
Figure 2. Bifurcation curves for EQ0. (a) $C_f - Re$ with different oscillation periods at $A_w^+ = 0.85$. Here wall units of the uncontrolled case at the saddle-node point are used for the scaling of the wall oscillation period. (b) $C_f - Re$ with different oscillation amplitudes at $T^+ = 79.8$. The arrow indicates the direction of increasing A_w^+. (c) $C_f - A_w^+$ with different oscillation periods at $Re = 400$. The red circle and triangle indicate two cases (A and B) of parameters for which the statistics are analysed.
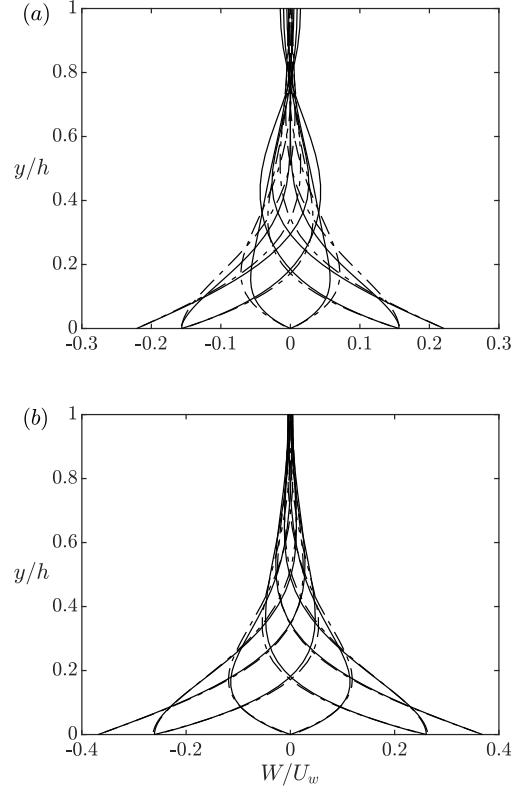

Figure 3. Spanwise Stokes layer for EQ0 and analytical solution at 8 equally separated phases. (a) Case A : $Re = 400$, $T^+ = 159.7$, $A_w^+ = 2.7$. (b) Case B : $Re = 400$, $T^+ = 159.7$, $A_w^+ = 4.5$.

Statistics

The spanwise wall oscillation form an unsteady near-wall spanwise shear layer (i.e. Stokes layer) that interacts with the near-wall structures. For the laminar case, the Stokes layer is represented analytically as (Schlichting, 1979)

$$W(y,t) = A_w e^{-\eta} \sin(2\pi t/T - \eta), \qquad (2)$$

where $\eta = -y\sqrt{\pi Re/T}$ drives the Stokes layer thickness which depends on the oscillation period. We note that the amplitude act on the spanwise displacement of the wall. In the laminar regime, the fluid enhanced by the spanwise wall oscillations and the streamwise flow are decoupled. Figure 3 shows the Stokes layer at 8 equally separated phases for the cases A and B indicated by the circle and triangle in figure 2(c), respectively. Here we fix the oscillation period $T^+ = 159.7$ and consider two amplitudes $A_w^+ = 2.7$ (case A) and $A_w^+ = 4.5$ (case B). The analytical Stokes layer deviates from the equilibrium state when the control is applied. We note that the deviation decreases when close to the wall and becomes substantial away from the wall. The Stokes layer of the equilibrium state is fixed by the wall-normal gradient of the spanwise Reynolds shear stress term $\partial \overline{v'w'}/\partial y$. The Reynolds shear stress has been found to increase with T^+ and Re (Ricco & Quadrio, 2008). Therefore, this justifies the improved agreement with the analytical solution when the Stokes layer is thin at small oscillation period T^+ (not shown here). We observe from figure 3 that the state with a higher drag (case A) differs significantly from the analytical solutions. Whereas, the state with a lower drag (case B) shows a quite good agreement even if the
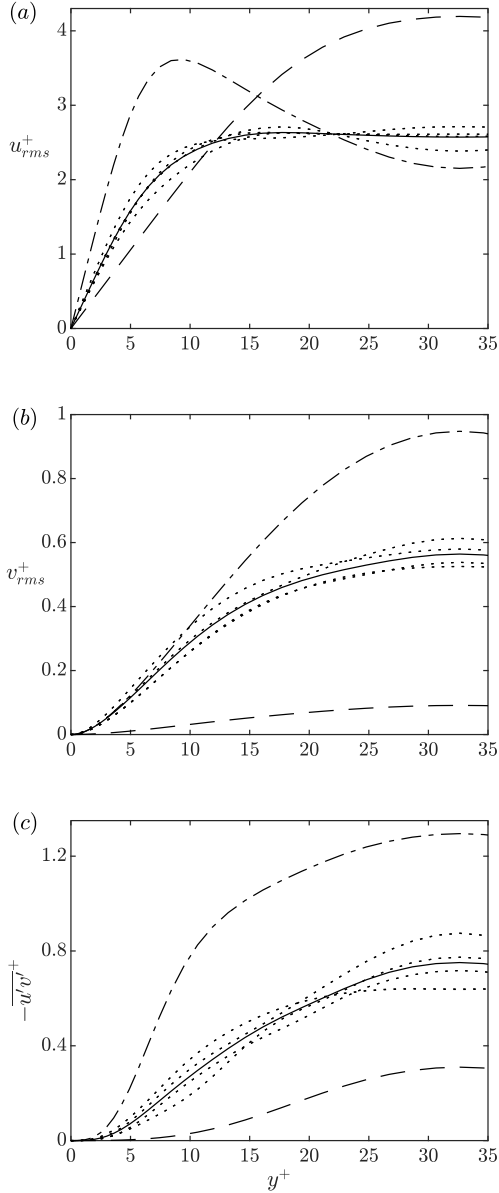
in terms of A_w^+. The critical A_w^+ of the saddle-node bifurcation is reached at lower values when the wall-oscillation period T^+ is increased.

3

Figure 4. Root mean square (r.m.s) velocity profiles for case A ($Re = 400$, $T^+ = 159.7$ and $A_w^+ = 2.7$). (a) u_{rms}^+, (b) v_{rms}^+, and (c) $-\overline{u'v'}^+$. The upper (lower) branch of the uncontrolled state is represented by dashed-dotted (dashed) lines. The controlled state is shown with dotted lines at 8 equally separated phases, and its mean profile is indicated by the solid line. The components are scaled with viscous inner units of the uncontrolled DNS.

amplitude of oscillations is twice smaller.

Figure 4 shows the root mean square (r.m.s) velocity components, u_{rms}^+, v_{rms}^+, and the streamwise shear stress $\overline{u'v'}^+$. The dotted lines indicate eight equally separated phases over one wall oscillation period. The peak in u_{rms}^+ of the upper branch is near the wall and that of the lower branch is located in the channel center. The profiles of state A (with $Re = 400$, $T^+ = 159.7$ and $A_w^+ = 2.7$) appear between the lower and upper branches. Compared to the upper branch, the state A shows an increase of u_{rms}^+ in the channel center and the near-wall peak observed in the upper branch is significantly weakened. Moreover, the control weakens the Reynolds shear stress $\overline{u'v'}^+$
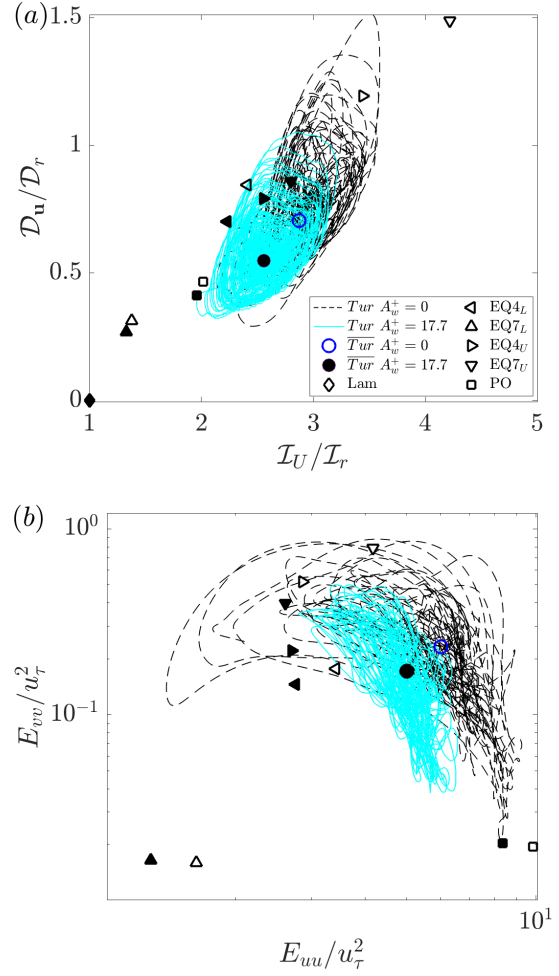

Figure 5. Phase portraits for controlled and uncontrolled states at $Re = 400$. The control parameters are set to $A_w^+ = 17.7$ and $T^+ = 14.3$. (a) $\mathscr{I}_U - \mathscr{D}_{\mathbf{u}}$ plane where D_r is the rate of total dissipation of the uncontrolled laminar state. (b) $E_{uu} - E_{vv}$ plane. The black dashed and solid cyan lines represent the controlled and uncontrolled turbulent states. The open and closed circles indicate the mean of those turbulent trajectories. The open and closed symbols show the uncontrolled and controlled equilibrium states, respectively. Each controlled equilibrium state is shown as the average over the wall-oscillation period.

compare to the upper-branch solution, which indicates a reduction of the drag according to the FIK identity (Fukagata *et al.*, 2002). Indeed the upper branch solution shows 35.8% of drag reduction. Those statistics features and bifurcation behaviour are similar to the other equilibrium solutions in the HKW box (not shown).

State-space dynamics

We will visualise and analyse, in this section, the state space using phase portraits. Following previous studies (e.g. Kawahara & Kida, 2001; Ibrahim *et al.*, 2019), we introduce the global mean kinetic energy (MKE):

$$\frac{dE_{\mathbf{U}}}{dt} = \underbrace{\frac{U_w \tau_{uw}}{h}}_{\mathscr{I}_U} - \underbrace{\frac{1}{V} \int_{\Omega} -\langle u'v'\rangle_{x,z} \frac{\partial U}{\partial y} dV}_{\mathscr{P}_{uv}} - \underbrace{\frac{\nu}{V} \int_{\Omega} \left(\frac{\partial U}{\partial y}\right)^2 dV}_{\mathscr{D}_U}$$

$$+ \underbrace{\frac{W_w \tau_{ww}}{h}}_{\mathscr{I}_W} - \underbrace{\frac{1}{V} \int_{\Omega} -\langle v'w'\rangle_{x,z} \frac{\partial W}{\partial y} dV}_{\mathscr{P}_{vw}} - \underbrace{\frac{\nu}{V} \int_{\Omega} \left(\frac{\partial W}{\partial y}\right)^2 dV}_{\mathscr{D}_W}$$

$$(3)$$

with the MKE given by

$$E_{\mathbf{U}} = \frac{1}{V} \int_{\Omega} \mathbf{U} \cdot \mathbf{U} \, dV, \qquad (4)$$

where Ω (Ω_N or Ω_{HKW}) is the given computational domain, U_w and W_w are the streamwise and spanwise velocities at the wall, and $\tau_{uw} = \nu\langle\partial U/\partial y|_{\pm h}\rangle_{x,z}$ and $\tau_{ww} = \nu\langle\partial W/\partial y|_{\pm h}\rangle_{x,z}$ the mean streamwise and spanwise shear stress, respectively. The average over the streamwise and spanwise directions is indicated by $\langle\cdot\rangle_{x,z}$. The terms, $\mathscr{I}_U$, $\mathscr{P}_{uv}$ and $\mathscr{D}_U$ in the first line of equation (3), are the rate of energy input, the rate of energy transport by streamwise mean shear to turbulent kinetic energy (TKE), and the dissipation rate by the streamwise mean velocity, respectively. Likewise, the three other terms in the second line, i.e. $\mathscr{I}_W$, $\mathscr{P}_{vw}$ and $\mathscr{D}_W$, correspond to the contributions from the spanwise wall oscillation. The volume-averaged equation of TKE writes as

$$\frac{dE_{\mathbf{u}}}{dt} = \underbrace{\frac{1}{V} \int_{\Omega} -\langle u'v'\rangle_{x,z} \frac{\partial U}{\partial y} dV}_{\mathscr{P}_{uv}}$$

$$+ \underbrace{\frac{1}{V} \int_{\Omega} -\langle v'w'\rangle_{x,z} \frac{\partial W}{\partial y} dV}_{\mathscr{P}_{vw}} - \underbrace{\frac{\nu}{V} \int_{\Omega} (\nabla \mathbf{u}')^2 dV}_{\mathscr{D}_{\mathbf{u}}} \qquad (5)$$

with $E_{\mathbf{u}} = E_{uu} + E_{vv} + E_{ww}$ is the total turbulent energy fluctuation averaged over the domain, written as

$$(E_{uu}, E_{vv}, E_{ww}) = \frac{1}{V} \int_{V} (u'^2, v'^2, w'^2)/U_w^2 dV, \qquad (6)$$

The first two terms, $\mathscr{P}_{uv}$ and $\mathscr{P}_{vw}$ in equation (5), are identical to those of (3), however in equation (5) they correspond to the rate of turbulence production by streamwise and spanwise mean shear. The last term $\mathscr{D}_{\mathbf{u}}$ is the turbulent kinetic energy dissipation. For details about the derivation of (3) and (5) in the context of spanwise wall oscillation in channel flow, the reader may refer to Ricco *et al.* (2012). Finally, the rate of total energy input and dissipation are given by $\mathscr{I} \equiv \mathscr{I}_U + \mathscr{I}_W$ and $\mathscr{D} \equiv \mathscr{D}_U + \mathscr{D}_W + \mathscr{D}_{\mathbf{u}}$, respectively.

We report in figure 5 the phase portraits in $\mathscr{D}_{\mathbf{u}}$ and the $E_{uu} - E_{vv}$ plane, respectively. We selected the solutions from Ω_{HKW} and we fix $Re = 400$ and the control parameters to $A_w^+ = 17.7$ and $T^+ = 14.3$. We present the equilibrium solutions and periodic edge state by averaging over a single wall-oscillation period while we show the turbulent state as time-dependent. Naturally, when the control is applied, non-zero
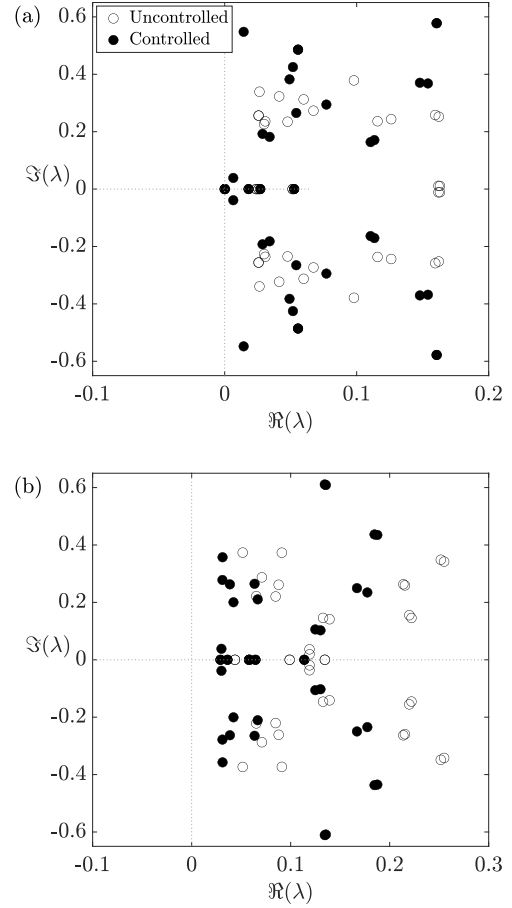

Figure 6. Spectra of complex-conjugate eigenvalues compared between uncontrolled and controlled ($A_w^+ = 17.7$, $T^+ = 14.3$) states. (a) the lower branch and (b) the upper branch of the equilibrium solution EQ4 at $Re = 400$.

spanwise energy input $\mathscr{I}_W$ feeds all the solutions (closed symbols). Figure 5(a) shows that the control pushes all the solutions towards the laminar state in the direction of decreasing $\mathscr{I}_U$ and $\mathscr{D}_{\mathbf{u}}$. Indeed, at these specific parameters, all the solutions indicate a reduction of drag (not shown). The upper branches and the mean turbulent state show a significant control effect compared to the lower solutions. Indeed, the lower branches EQ4$_L$ and EQ7$_L$ show 7.3% and 3.2% of drag reduction (DR), and the upper branches EQ4$_U$ and EQ7$_U$ show 25.8% and 33.7% of DR respectively, and the mean turbulent state indicates 10.9% of DR. The phase portrait in $E_{uu} - E_{vv}$ plane shown in figure 5(b) indicates similar results. The decrease in E_{vv} is the consequence of a reduction in the wall-normal velocity fluctuation resulting from the control and pushing the solutions towards the laminar state. Generally, the control significantly affects the upper branches and has only a modest effect on the lower branches. The phase portraits indicate that the spanwise wall oscillation reduces the spread of the turbulent state in phase space. Furthermore, the state-space distances between the upper and lower branch of each solution are reduced, indicating stabilisation of turbulence.

More generally, Figure 5 shows a reduction in the size of the turbulent state region in state-space. This observation may indicate that the control damps the repelling strength of each equilibrium. Therefore, we further investigate this reduction in the turbulent state region by checking the eigenspectra of the
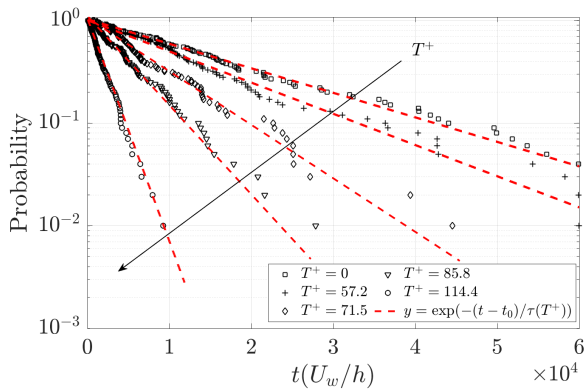
5

Figure 7. Probability distribution of turbulence to sustain over time at $Re = 400$ and $A_w^+ = 1.2$ for different values of wall oscillation period T^+. The square symbols indicate the uncontrolled reference case at $A_w^+ = 0$. The black arrow indicates the increasing direction of T^+.

exact coherent states. Figure 6 shows the complex-conjugate eigenvalues of the lower and upper branches of EQ4. The real and imaginary parts indicate the growth rate and frequency of the eigenmodes, respectively. The lower branch solutions show a small drag reduction (or even drag increase) and pair with a negligible influence on the growth rates of the leading eigenmodes, indicating a weak effect of spanwise wall oscillation control. However, we observe for the upper branch solutions of both cases, that the growth rates of the eigenmodes follow that of the drag when control is active. Indeed, the growth rate decreases where the control provokes a reduction of drag, indicating a stabilisation.

Turbulence in Couette flow with the given flow domains is known as a 'chaotic saddle', and it is characterised by finite lifetime (Eckhardt et al., 2007a). The lifetime of the uncontrolled turbulent state also increases very rapidly with the Reynolds number (Eckhardt et al., 2007b). The state-space characteristics discussed in figures 5 and 6 suggest a strong similarity between the effect of the control and that of lowering the Reynolds number, indicating a reduction of turbulence lifetime when control is active. Therefore, the overall influence of the state space by the spanwise wall oscillation is finally examined by computing the lifetime of turbulence subject to the given control. To evaluate the lifetime, we carried out groups of 100 controlled and uncontrolled DNS at $Re = 400$. The initial conditions of the simulations were first obtained from 100 states computed at a slightly higher Reynolds number, $Re = 415$. The lifetime is defined as a probability distribution for the amplitude $A_w^+ = 1.2$ and oscillation periods $T^+ = 57.2$, 71.5, 85.8, and 114.4. To monitor the lifetime of each simulation, we fix a threshold of the turbulent energy fluctuation $E_{vv} + E_{uu} < 10^{-5}$, below which turbulence will decay to laminar flow. Figure 7 shows the probability for turbulence to sustain up to a given time t as a function of A_w^+ and T^+. We first observe the classic exponential distribution of the lifetime, confirming that this is a memoryless process (Eckhardt et al., 2007a). It is found that the spanwise wall oscillation significantly reduces the lifetime of turbulence at $A_w^+ = 1.2$, as the wall-oscillation period T^+ is increased. The control clearly enhances flow relaminarisation.

Conclusion

We investigated, in this study, the effect of spanwise wall oscillation control on exact coherent states computed in two different domains. We found that the upper branches of the solutions are stabilized, and their skin-friction drag is reduced. On the other hand, the lower branches are merely affected by the control. The stabilisation of the upper-branch solution translates by the movement of the saddle-node bifurcation point of the solutions to higher Reynolds numbers. When we vary the oscillation amplitude, this behaviour is observed for all the solutions. However, when varying T^+, such a trend is reversed for EQ0 when $T^+ \geq 100$, consistent with the observation in the previous DNS. We observed in the phase portraits that the spanwise wall oscillation reduces the size of the state space region as well as the repelling strength of the upper-branch equilibrium states. The change in the state-space dynamics relates to the significant turbulence lifetime decrease. Finally, the suppression of the lift-up effect may be the principal stabilisation mechanism of exact coherent structures.

Acknowledgments

REFERENCES

Bewley, T. R. 2014 Numerical renaissance: Simulation, optimisation and control. *Renaissance Press* .

Butler, K. M. & Farrell, B. F. 1993 Optimal perturbations and streak spacing in wall-bounded turbulent shear flow. *Phys. Fluids* **5**, 774–777.

Eckhardt, B., Schneider, T.M., Hof, B. & Westerweel, J. 2007a Turbulence Transition in Pipe Flow. *Ann. Rev. Fluid Mech.* **39**, 447.

Eckhardt, B., Schneider, T. M., Hof, B. & Westerweel, J. 2007b Turbulence transition in pipe flow. *Ann. Rev. Fluid Mech.* **39**, 447–468.

Fukagata, K., Iwamoto, K. & Kasagi, N. 2002 Contribution of Reynolds stress distribution to the skin friction in wall-bounded flows. *Phys. Fluids* **14** (11), L73–L76.

Gibson, John F, Halcrow, Jonathan & Cvitanović, Predrag 2009 Equilibrium and travelling-wave solutions of plane couette flow. *J. Fluid Mech.* **638**, 243–266.

Hamilton, James M., Kim, John & Waleffe, Fabian 1995 Regeneration mechanisms of near-wall turbulence structures. *J. Fluid Mech.* **287**, 317–348.

Ibrahim, Joseph I, Yang, Qiang, Doohan, Patrick & Hwang, Yongyun 2019 Phase-space dynamics of opposition control in wall-bounded turbulent flows. *J. Fluid Mech.* **861**, 29–54.

Jung, W.-J., Mangiavacchi, N. & Akhavan, R. 1992 Suppression of turbulence in wall-bounded flows by high-frequency spanwise oscillations. *Phys. Fluids A* **4** (8), 1605–1607.

Kawahara, Genta 2005 Laminarization of minimal plane couette flow: going beyond the basin of attraction of turbulence. *Phys. Fluids* **17** (4), 041702.

Kawahara, G. & Kida, S. 2001 Periodic motion embedded in plane Couette turbulence: regeneration cycle and burst. *J. Fluid Mech.* **449**, 291–300.

Kravchenko, A. G., Choi, H. & Moin, P. 1993 On the relation of near-wall streamwise vortices to wall skin friction in turbulent boundary layers. *Phys. Fluids A* **5**, 3307.

Nagata, M. 1990 Three-dimensional finite-amplitude solutions in plane Couette flow: bifurcation from infinity. *J. Fluid Mech.* **217**, 519–527.

Ricco, P., Ottonelli, C., Hasegawa, Y. & Quadrio, M. 2012 Changes in turbulent dissipation in a channel flow with oscillating walls. *J. Fluid Mech.* **700**, 77–104.

Ricco, P. & Quadrio, M. 2008 Wall-oscillation conditions for drag reduction in turbulent channel flow. *Intl J. Heat Fluid Flow* **29** (4), 891–902.

Ricco, Pierre, Skote, Martin & Leschziner, Michael A 2021 A review of turbulent skin-friction drag reduction by near-wall transverse forcing. *Prog. Aerosp. Sci* **123**, 100713.

Schlichting, H. 1979 *Boundary-Layer Theory*. New York: Mc Graw-Hill.

Yang, Q., Willis, A. P. & Hwang, Y. 2019 Exact coherent states of attached eddies in channel flow. *J. Fluid Mech.* **862**, 1029–1059.